



In vivo monitoring platform of transplanted human stem cells using magnetic resonance imaging

Seungmin Han^{a,b,1}, Byunghoon Kang^{a,c,1}, Hye Young Son^{d,e}, Yuna Choi^d, Moo-Kwang Shin^a, Jongjin Park^f, Jeong-Ki Min^{f,g}, Daewon Park^h, Eun-Kyung Lim^{c,j,**}, Yong-Min Huh^{d,e,i,***}, Seungjoo Haam^{a,*}

^a Department of Chemical and Biomolecular Engineering, Yonsei University, 50 Yonsei-ro, Seodaemun-gu, Seoul, 03722, Republic of Korea

^b Division of Cardio-Thoracic Surgery, Department of Surgery, College of Medicine, University of Arizona, Tucson, AZ, USA

^c BioNanotechnology Research Center, Korea Research Institute of Bioscience and Biotechnology (KRIBB), 125 Gwahak-ro, Yuseong-gu, Daejeon, 34141, Republic of Korea

^d Department of Radiology, College of Medicine, Yonsei University, 50-1 Yonsei-ro, Seodaemun-gu, Seoul, 03722, Republic of Korea

^e Severance Biomedical Science Institute, College of Medicine, Yonsei University, 50-1 Yonsei-ro, Seodaemun-gu, Seoul, 03722, Republic of Korea

^f Biotherapeutics Translational Research Center, Korea Research Institute of Bioscience and Biotechnology (KRIBB), 125 Gwahak-ro, Yuseong-gu, Daejeon, 34141, Republic of Korea

^g Department of Biomolecular Science, KRIBB School of Bioscience, University of Science and Technology (UST), 217 Gajeong-ro, Yuseong-gu, Daejeon, 34141, Republic of Korea

^h Bioengineering Department, University of Colorado Denver Anschutz Medical Campus, Aurora, CO, USA

ⁱ YUHS-KRIBB Medical Convergence Research Institute, 50-1 Yonsei-ro, Seodaemun-gu, Seoul, 03722, Republic of Korea

^j Department of Nanobiotechnology, KRIBB School of Biotechnology, University of Science and Technology (UST), 217 Gajeong-ro, Yuseong-gu, Daejeon, 34113, Republic of Korea

ARTICLE INFO

Keywords:

Stem cell therapy
Stem cell monitoring
In vivo MR monitoring
Hollow MnO nanoparticle
Human anti-integrin $\beta 1$ antibody

ABSTRACT

As stem cells show great promise in regenerative therapy, stem cell-mediated therapeutic efficacy must be demonstrated through the migration and transplantation of stem cells into target disease areas at the pre-clinical level. In this study, we developed manganese-based magnetic nanoparticles with hollow structures (MnOHo) and modified them with the anti-human integrin $\beta 1$ antibody (MnOHo-Ab) to enable the minimal-invasive monitoring of transplanted human stem cells at the pre-clinical level. Compared to common magnetic resonance imaging (MRI)-based stem cell monitoring systems that use pre-labeled stem cells with magnetic particles before stem cell injection, the MnOHo-Ab is a new technology that does not require stem cell modification to monitor the therapeutic capability of stem cells. Additionally, MnOHo-Ab provides improved T1 MRI owing to the hollow structure of the MnOHo. Particularly, the anti-integrin $\beta 1$ antibody (Ab) introduced in the MnOHo targets integrin $\beta 1$ expressed in the entire stem cell lineage, enabling targeted monitoring regardless of the differentiation stage of the stem cells. Furthermore, we verified that intravenously injected MnOHo-Ab specifically targeted human induced pluripotent stem cells (hiPSCs) that were transferred to mice testes and differentiated into various lineages. The new stem cell monitoring method using MnOHo-Ab demonstrates whether the injected human stem cells have migrated and transplanted themselves in the target area during long-term stem cell regenerative therapy.

* Corresponding author.

** Corresponding author. BioNanotechnology Research Center, Korea Research Institute of Bioscience and Biotechnology (KRIBB), 125 Gwahak-ro, Yuseong-gu, Daejeon, 34141, Republic of Korea.

*** Corresponding author. Department of Radiology, College of Medicine, Yonsei University, 50-1 Yonsei-ro, Seodaemun-gu, Seoul, 03722, Republic of Korea.

E-mail addresses: eklim1112@kribb.re.kr (E.-K. Lim), ymhuh@yuhs.ac (Y.-M. Huh), haam@yonsei.ac.kr (S. Haam).

¹ These authors contributed equally to this work.

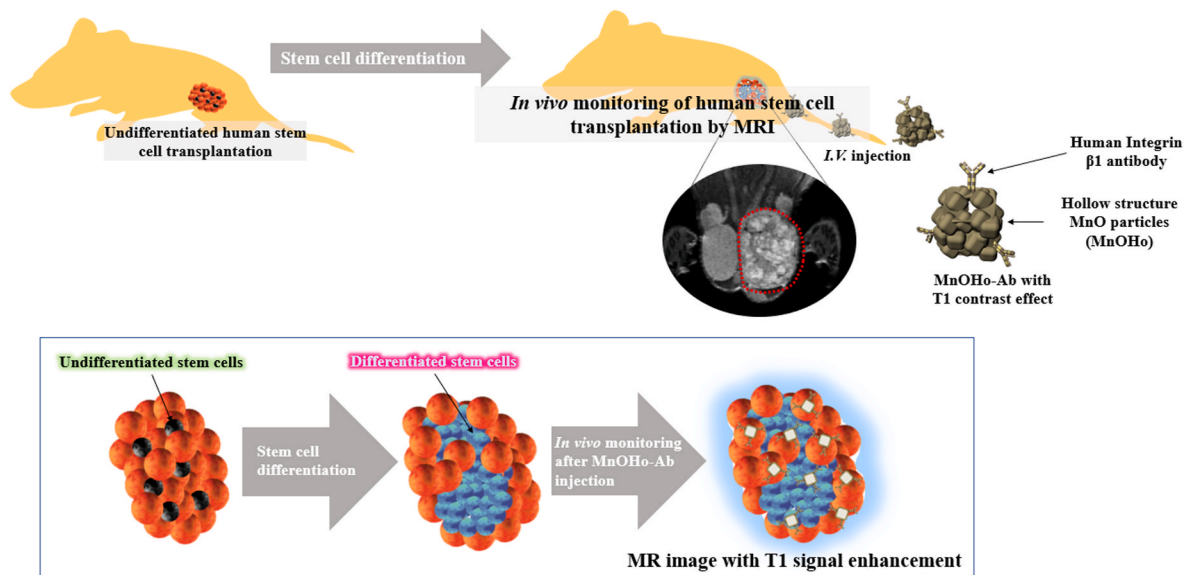


Fig. 1. Schematic illustration of the MR monitoring system using hollow structured MnO nanoparticles, incorporating antibodies, targeting a specific integrin (integrin $\beta 1$) (MnOho-Ab) to assess human stem cell transplantation. MnOho-Ab is able to target and monitor human stem cells differentiated in any lineage after transplantation.

1. Introduction

Stem cells, that can renew themselves and differentiate into various cell types in the body, have a natural ability to repair injured or diseased tissue by replacements of cells (Zakrzewski et al., 2019). Adoptive stem cell transfer therapy has been widely applied in clinical trials and has been considered a promising field in tissue regenerative therapy (Jarbaek Nielsen et al., 2020; Rajabzadeh et al., 2019; Zakrzewski et al., 2019). Various developments have enhanced the therapeutic efficacy of stem cells by overcoming drawbacks such as human induced pluripotent stem cells (hiPSCs)-derived adult stem cells to ensure the limited proliferation and the induction of homing receptors for low migration rates (Doi et al., 2020; Hwang et al., 2008; Lian et al., 2010; Won et al., 2014). The developed stem cells need to be investigated for safety and efficacy at the pre-clinical level before clinical application. However, there are many unanswered questions regarding whether the therapeutic efficacy results from stem cell differentiation or the peripheral effect of stem cells, as only 1–2% of the adoptively transferred stem cells reach the target tissue, and the remaining are lost in a few days at the pre-clinical level (Bulte and Daldrop-Link 2018; Li et al., 2016; McGinley et al., 2013; Zhang et al., 2001). There is a need for technology to demonstrate the effects of stem cell-mediated therapy at the pre-clinical level without animal sacrifice. Thus, the migration and transplantation of stem cells are confirmed using minimal-invasive imaging techniques by directly labeling them with a high-sensitivity imaging probe or indirectly labeling them through gene insertion (Bulte and Daldrop-Link 2018; Cen et al., 2016; Rodriguez-Porcel 2010; Wang et al., 2011). Among various imaging techniques, magnetic resonance imaging (MRI)-based methods have advantages owing to their high spatial resolution, enabling detailed cell tracking (Barsanti et al., 2015; Panagiotopoulos et al., 2015; Rodriguez-Porcel 2010). To date, magnetic nanoparticles (MNPs) have modified stem cells by internalization or attachment to stem cells prior to animal transplantation to monitor stem cells using MRI (Ariza de Schellenberger et al., 2016; Liu et al., 2016; Mathiasen et al., 2019; Shahrer et al., 2019). However, these methods have several issues. First, uncertainty to bring maximum effect of stem cell-mediated therapeutic capability because of cell-modification. In addition, unpredictability of the signal from the MNPs to tell whether the stem cells are alive or well-transplanted because of pre-bound of MNPs to stem cells, and also signal decrease caused by diminished particle-to-cell density during *in*

vivo cell proliferation (Bulte and Daldrop-Link 2018; Rodriguez-Porcel 2010; Santos and Yang 2016).

To harness the therapeutic capability of stem cells and overcome the limitations mentioned above, we suggest a new strategy to monitor the stem cells transferred *in vivo* at the pre-clinical level using stem cell-targeted MRI probes, namely the anti-human integrin $\beta 1$ antibody-modified MNPs. Integrin $\beta 1$ is ubiquitously expressed in the overall lineage of stem cells and has been reported as an essential factor for cell adhesion. Therefore, this strategy can monitor the transplanted human stem cells based on antibody-cell interaction (Chen et al., 2013; Kallas-Kivi et al., 2018; Prowse et al., 2011). While the deficiency of integrin $\beta 1$ results from cell implantation, homing and migration failure, high integrin $\beta 1$ expression appears when stem cells are transplanted and integrated into the tissue for regeneration (Clark et al., 2020; Ip et al., 2007; Xiong et al., 2020). As integrin $\beta 1$ expression continuously increases as the transferred stem cells proliferate and transplant, this method allows *in vivo* monitoring during stem cell differentiation (Li et al., 2017; Prowse et al., 2011). A hollow manganese-based MNP (MnOho) that we developed and optimized to obtain an improved T1 signal was utilized as a stem cell-targeted MRI probe in this study (Kukreja et al., 2020). Manganese-based particles (MnO) have been developed as promising alternatives to gadolinium(III) (Gd^{3+}), a gold-standard contrast agent for MRI, because MnO particles show higher T1 relaxation and lower toxicity compared to gadolinium (Addisu et al., 2018; Aime et al., 2002; Idée et al., 2009; Pan et al., 2011). We modified the MnOho with an anti-human integrin $\beta 1$ antibody (MnOho-Ab) to monitor *in vivo* stem cell-based regenerative therapy. We transplanted hiPSCs in mice to assess the *in vivo* monitoring of MnOho-Ab as a proof-of-concept because iPSCs can differentiate into diverse types of adult stem cells. The intravenously injected MnOho-Ab successfully targeted the transplantation of human stem cells and showed a distinguishable T1 signal even in the early stages of transplantation (Fig. 1). The advantage of our strategy is that stem cells can be administered without any modification to enable monitoring, allowing them to induce their therapeutic capacity fully. Specifically, MnOho-Ab can confirm that stem cells have been implanted *in vivo* with high-resolution images, and no direct cell modification is required.

Therefore, it can be used for monitoring of stem cells by intravenously injecting it during stem the administration of cell regenerative therapy. We believe that MnOho-Ab has the potential to be a new

strategy for monitoring stem cells at the pre-clinical level in stem cell therapy.

2. Materials and methods

2.1. Materials

Manganese(II) formate ($\text{Mn}(\text{COOH})_2$), tri-n-octylamine (TOA), oleic acid (OA), polyacrylic acid (PAA), diethylene glycol (DEG), N-(3-Dimethylaminopropyl)-N-ethylcarbodiimide hydrochloride (EDC), and basic fibroblast growth factor (bFGF) were procured from Sigma-Aldrich. N-hydroxysulfosuccinimide (NHS) was purchased from Thermo Fisher Scientific. Anti-integrin beta (β) 1 antibody (12G10) (Ab) was obtained from Abcam. Dulbecco modified Eagle medium (DMEM)/F-12, DMEM, knockout serum replacement (KSR), MEM non-essential amino acid (NEAA) solution, antibiotic-antimycotic (A-A), and β -mercaptoethanol (Gibco®) were purchased from Thermo Fisher Scientific. Ethanol, chloroform, and phthalate buffer (pH 4.0) were obtained from Samchun Chemical. All other reagents purchased from commercial sources were used as obtained without further purification. Ultrapure deionized water was used for all the synthetic processes.

2.2. Synthesis of MnOHO and MnOHO-Ab

$\text{Mn}(\text{COOH})_2$ (1 mmol) was added to a mixture containing 3 mmol of TOA and 3 mmol of OA. This mixture was heated in a vacuum to 130 °C until the moisture was completely removed. This mixture was heated at 270 °C for 1 h and refluxed at 330 °C until the color changed from brownish red to green. The mixture was kept under a flow of N_2 for 1 h and then cooled to 15 °C to obtain uniform MnO nanoparticles. The resulting particles were precipitated after adding ethanol by centrifugation at 6000 rpm for 10 min. They were washed twice with hexane and ethanol and finally dispersed in hexane. A ligand exchange reaction was performed to modify the surface of the hydrophobic oleate-capped MnO particles. Further, a solution containing 20 mL of DEG and 200 mg of PAA was heated in a vacuum to 140 °C for 1 h with magnetic stirring. The mixture was then refluxed under N_2 for 2 h at 200 °C. A solution of 40 mg of MnO nanoparticles in 4 mL of hexane was quickly added to the same flask, and this reactant was maintained at 200 °C for an additional 6 h. After cooling to room temperature, the resulting nanoparticles were precipitated by adding ethanol and then collected by centrifugation. Finally, the ligand-exchanged-MnO particles were dissolved in the aqueous phase. We observed successful phase transference of the ligand-exchanged-MnO particles (from hexane to buffer) after the surface ligand exchange occurred from OA to PAA. Then, 10 mg of the ligand-exchanged-MnO particles were dispersed into 20 mL of phthalate buffer (pH 4.0) and stirred for 12 h to carve away the MnO core. The resulting MnOHO were obtained by centrifugation and were resuspended in deionized water. EDC (50 mg), sulfo-NHS (20 mg), and Ab were added to 10 mL of the MnOHO (1 mg/mL) and reacted overnight at 4 °C to modify the MnOHO with anti-human integrin β 1 antibody (Ab). Unwanted products were removed after the reaction using centrifugation, and the resulting MnOHO-Ab particles were obtained by re-dispersing them in 4 mL of PBS (Gibco® Dulbecco's Phosphate-Buffered Saline).

2.3. Cell culture

For this study, human iPSCs (hiPSCs) were purchased from ATCC (ATCC-DYR0100 Human Induced Pluripotent Stem Cells (ATCC® ACS-1011), Manassas, VA, USA). Mouse embryonic fibroblast cells (MEFs) were manually obtained from mouse embryos (Jiang et al., 2016). HiPSCs were cultured on feeder cell layers made from MEFs and were maintained in knockdown DMEM/F-12 containing 20% KSR, 1% MEM NEAA solution, 1% A-A, 0.1% bFGF, and 0.2% β -mercaptoethanol. MEFs were cultured in DMEM containing 10% fetal bovine serum (Welgene

Inc.) and 1% A-A. Feeder cells were prepared by treating MEFs with mitomycin C (MMC, Roche Inc.). All cell lines were incubated at 37 °C under 5% CO_2 .

2.4. Characterization of MnOHO and MnOHO-Ab

The shapes and sizes of the MnOHO and MnOHO-Ab were analyzed using transmission electron microscopy (TEM; JEM-F200, JEOL Ltd.) and laser scattering (ELS-Z, Otsuka Electronics), respectively. The crystallinities of all the particles (MnO, MnOHO, and MnOHO-Ab) were determined using X-ray diffraction (XRD; Rigaku, X-ray Diffractometer Ultima3) at 298 K. Their magnetic properties were also analyzed using a vibrating sample magnetometer (VSM; MODEL-7407, Lakeshore) at 298 K. T1-weighted MRI experiments were performed using a 3.0 T clinical MRI scanner with a micro-47 surface coil (Intera; Philips Medical Systems, Best, the Netherlands). The R1 relaxivity of the MnOHO-Ab was measured using the Carr-Purcell-Meiboom-Gill pulse sequence at room temperature with the following parameters: echo time (TE) = 60 ms, repetition time (TR) = 4000 ms, slice thickness = 2.0 mm, number of acquisitions = 1, and point resolution = $234 \times 234 \mu\text{m}^2$. Relaxivity values, R1, were calculated using a series of T1 values when plotted as $1/\text{T1}$ versus Mn concentrations. The relaxivity coefficient ($\text{mM}^{-1} \text{s}^{-1}$) was equal to the ratio of R1 ($1/\text{T1}, \text{s}^{-1}$) to the concentration of each nanoparticle. We also measured the T1-weighted MR image of the MnOHO and its relaxivity in the same manner.

2.5. Cytotoxicity assay of MnOHO-Ab

The cytotoxicity of the MnOHO-Ab on the hiPSCs was assessed using a 3-(4,5-dimethyl thiazolyl-2)-2,5-diphenyl tetrazolium bromide (MTT) assay by measuring the degree of cell growth inhibition. HiPSCs (1×10^4) were plated on 96-well plates and incubated for 24 h at 37 °C under a humidified atmosphere containing 5% CO_2 . The hiPSCs were then incubated overnight with various concentrations of MnOHO-Ab containing culture medium without KSR. The cells were washed in triplicate using Dulbecco's phosphate-buffered saline (DPBS) to wash out the unbound MnOHO-Ab. In the MTT assay performed as per the standard methods, the yellow tetrazolium salt was transformed into purple formazan crystals in the metabolically activated cells. The relative percentage of cell viability was calculated as the ratio of formazan intensity in viable cells treated with MnOHO-Ab compared to that in the untreated cells. The results are presented as the average \pm standard deviation ($n = 6$).

2.6. In vitro targeting ability of MnOHO-Ab

First, the binding affinity of only Ab against each cell (hiPSCs and MEFs) was confirmed by FACS analysis. Each cell was incubated with Ab for 1 h at 4 °C and then washed with PBS to remove unbound free Ab. In subsequent, PE-tagged secondary antibody was utilized to label bound-Ab. After that, *in vitro* targeting ability of the MnOHO-Ab was confirmed using TEM imaging and MRI. For the TEM of the cells, MEFs and hiPSCs were first seeded onto a six-well plate, incubated overnight at 37 °C with 5% CO_2 , and then treated with 2 mM MnOHO-Ab. After incubation for 1 h at 37 °C, the cells were washed three times with PBS to rinse out the unbound nanoparticles and then were harvested and fixed with a fixation buffer. The sample was submitted to Yonsei Medical College for sample embedding and tissue sectioning. The sections obtained were stained with 6% uranyl acetate staining solution for 20 min and with citrate buffer (pH 6.0) (Thermo Fisher Scientific) for 10 min for contrast staining. The stained cellular TEM sample was observed by TEM (JEOL-1011). Cell MRI was conducted using a 3.0 T clinical MRI instrument with a wrist coil. MEFs and hiPSCs were collected and incubated with various concentrations of MnOHO and MnOHO-Ab (2 mM and 10 mM) for 1 h at 4 °C to reduce nonspecific binding effects. The cells were then washed five times with DPBS to eliminate unbound MnOHO and

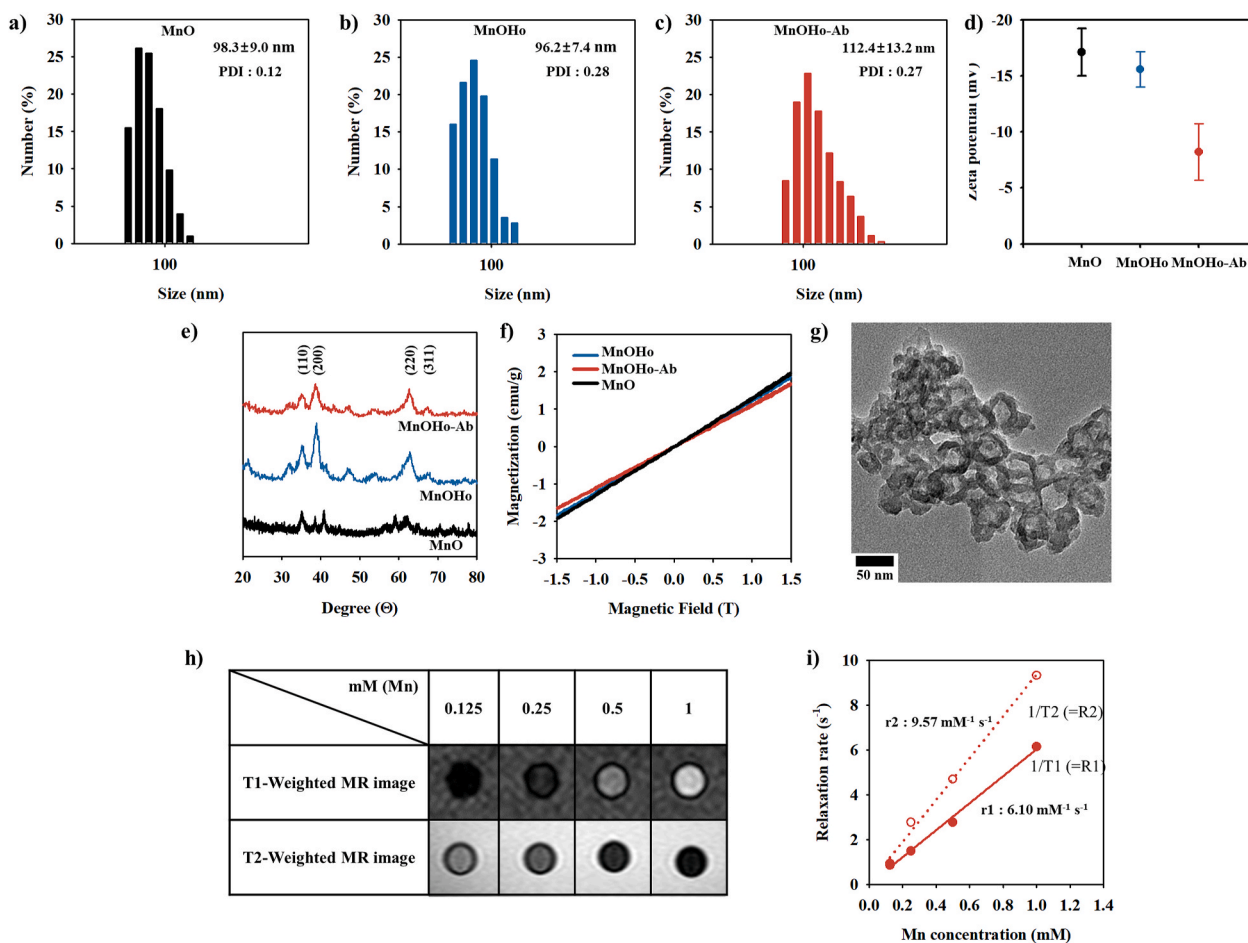


Fig. 2. Characteristic analysis of MnO and MnOHo-Ab. (a), (b) and (c) present the size distribution histogram of MnO, MnOHo and MnOHo-Ab, respectively, obtained using dynamic light scattering analysis. (d) presents their zeta-potential values, (e) their X-ray diffraction (XRD) patterns, and (f) their Magnetic hysteresis loop, analyzed using a vibrating sample magnetometer (VSM). (g) TEM images of MnOHo-Ab. (h) T1-weighted and T2-weighted MRI images depending on Mn^{2+} concentration of MnOHo-Ab. (i) Plots of each relaxation ($1/T_1$ and $1/T_2$) against the Mn^{2+} concentration of MnOHo-Ab. Mn concentration was calculated based on ICP-AES.

MnOHo-Ab. Finally, the cells were fixed in 4% paraformaldehyde (PFA) solution and taken for MRI screening.

2.7. In vivo modeling (stem cell transplantation) procedure

All animal experiments were performed with the approval of the Institutional Animal Care and Use Committee of Yonsei University Health System. HiPSCs were detached using StemPro® EZpassage™ (Invitrogen, USA). Approximately 8×10^6 cells of hiPSCs were transplanted by direct injection into male mouse testes. These hiPSC-implanted mice were then subjected to weekly T1-weighted MRI to confirm teratoma formation.

2.8. In vivo MR imaging

We performed *in vivo* MRI experiments using a 3 T clinical MRI instrument with a wrist coil (Intera; Philips Medical Systems, Best, The Netherlands). The mice were first intravenously administered 200 μL of MnOHo and MnOHo-Ab (10 mg/mL). The bio-distribution of particles was monitored using MR images at various times after particle injection (post-injection, 1 h, 2 h, and 4 h). Additionally, during the 6 weeks of teratoma formation, the mice were administered MnOHo-Ab weekly and monitored using MRI. For T1-weighted MRI in mice with teratoma formation, we utilized the following parameters: point resolution = $0.234 \text{ mm} \times 0.234 \text{ mm}$, section thickness = 1.0 mm, TE = 12.7 ms, TR

= 694 ms, and the number of acquisitions = 1.

2.9. Ex vivo experiments

After MnOHo injection, the *in vivo* toxicity of the MnOHo was confirmed using hematoxylin and eosin (H&E) staining for each organ (brain, heart, kidney, liver, spleen, and testis). Additionally, most organs of the mice injected with MnOHo-Ab were excised after obtaining *in vivo* MRI images and kept in the fixation buffer (4% PFA solution). Selected organs were lyophilized to remove moisture, and the mass of each organ was measured. We analyzed the Mn ion concentration in each organ using inductively coupled plasma atomic emission spectrometry (ICP-AES). Particularly, normal testicular tissue and that with teratoma formation were excised and embedded in paraffin. The paraffin-embedded tissues were sectioned and stained with H&E. All the stained tissue slides were analyzed using a virtual slide microscope (Olympus VS120, Japan) and the Olyvia software.

2.10. Statistical analysis

All the data presented in this study represent biological triplicate experiments, with each experiment yielding comparable results. Statistical p-value was analyzed with one-way ANOVA or two-way ANOVA with Tukey's tests using GraphPad Prism 8 software. The statistical significance threshold of each test was set at $P < 0.05$: * < 0.05 , ** $<$

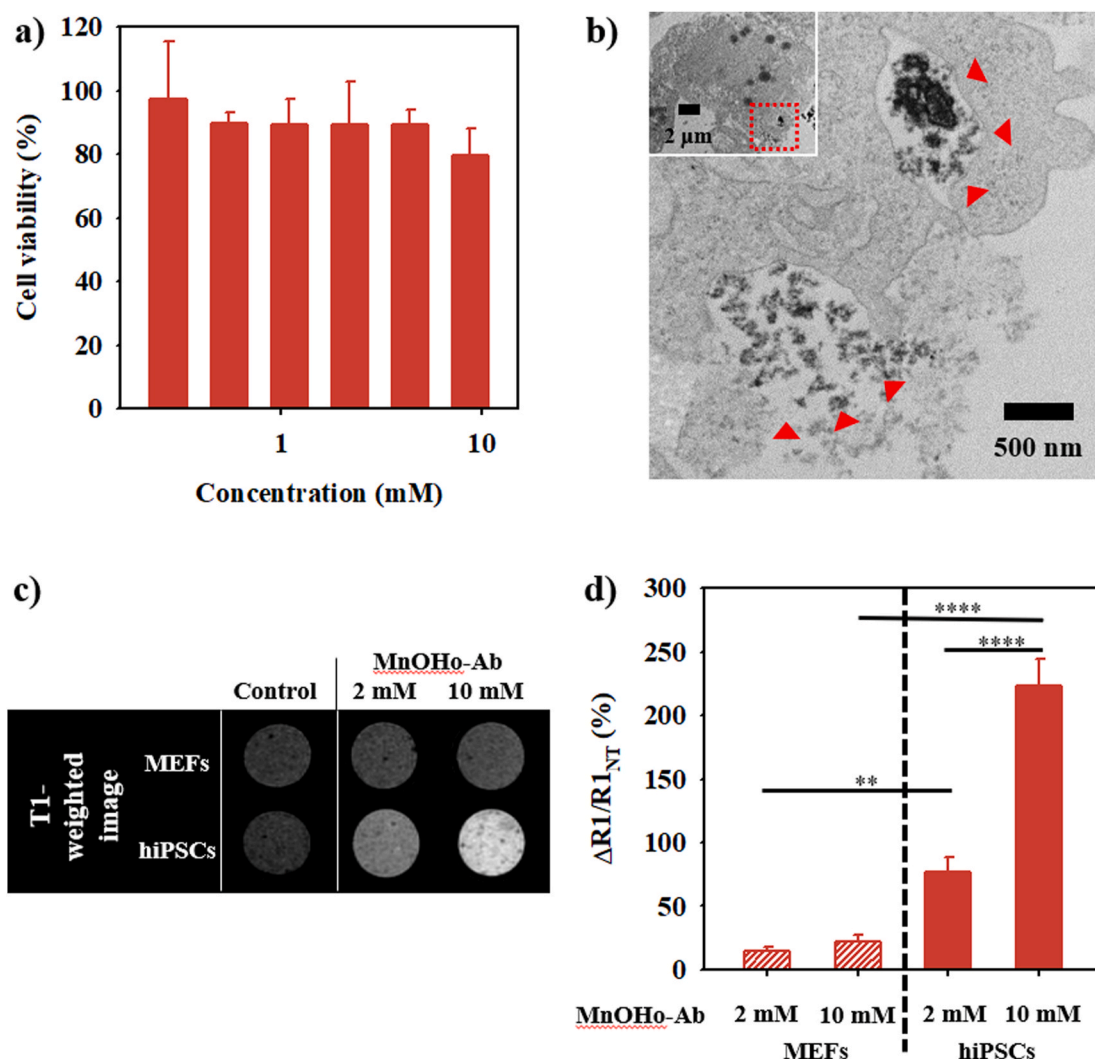


Fig. 3. Cellular interaction and hiPSCs specific binding affinity of MnOHO-Ab. (a) The Viability of hiPSCs incubated with MnOHO-Ab at various concentrations for 24 h at 37 °C. (b) Cellular TEM images of hiPSCs treated with MnOHO-Ab for 1 h; Red arrow indicates MnOHO-Ab in the endocytosis process. (c) T1-weighted MRI images of MnOHO-Ab-treated MEFs and hiPSCs. The cells were treated with MnOHO-Ab for 1 h. (d) Relative signal intensity ($\Delta R1/R1_{NT}$ (%)) graphs of hiPSCs and MEFs incubated with MnOHO-Ab (2 and 10 mM) ($\Delta R1 = R1 - R1_{NT}$, NT: no treatment). Data represented is the mean \pm SD (** < 0.01, **** < 0.0001, one-way ANOVA with Tukey's tests). (e) The relative signal intensity value of each cell. (For interpretation of the references to color in this figure legend, the reader is referred to the Web version of this article.)

0.01, *** < 0.001, and **** < 0.0001.

3. Results and discussion

A highly sensitive MRI probe is required to monitor adoptive stem cell transfer at the pre-clinical level, which can very sensitively detect stem cells *in vivo*. Therefore, we developed MnOHO-Ab for highly sensitive T1-weighted MRI. To ensure the high sensitivity of MnOHO, monodispersed MnO was first generated before producing MnOHO following our previous study (Fig. S1) (Kukreja et al., 2020). The MnOHO had an increased surface area by modifying MnO's interior into a hollow structure, which could increase the T1 enhancement effect by enlarging the contact area between the water proton and metal ion of the particle surface. Then, MnOHO-Ab was prepared by chemically binding the anti-human integrin $\beta 1$ antibody (Ab) to PAA on the particle surface. It was confirmed that this Ab we used exhibited high binding affinity for hiPSC compared to MEFs by FACS analysis (Fig. S2). Additionally, as a result of labeling the synthesized MnOHO (10 mg) with an integrin antibody (10 μ g), it was confirmed that MnOHO-Ab having an Ab of 3.5 μ g was generated through Bradford assay.

The particles' size distribution and dispersion stability in the aqueous solution were analyzed using dynamic light scattering analysis and zeta potential measurements. MnOHO was found to be about 96.2 ± 7.4 nm in size, with a strong negative charge due to the presence of carboxyl groups of PAA on its surface. In comparison, MnOHO-Ab had an increased size of about 112.4 ± 13.2 nm, and its surface charge was close to neutral due to antibody modification on the carboxyl groups of PAA (Fig. 2a–d). Further, the XRD results of MnO, MnOHO, and MnOHO-Ab showed that the crystalline peaks matched the series of Bragg reflections corresponding to the standard and phase-pure cubic rock salt structure of MnO ($a = 4.442$ Å), indicating that they maintained crystallinity regardless of ligand exchange and surface modification (Fig. 2e). The field-dependent magnetization curves for MnOHO and MnOHO-Ab exhibited magnetization values of 1.86 and 1.68 emu/g, respectively, at an external magnetic field of 1.5 T with no remanence coercivity at zero fields. This indicated that MnOHO-Ab retained its paramagnetic properties at room temperature regardless of the antibody, compared to MnOHO (Fig. 2f). Fig. 2f shows the hollow structure of MnOHO-Ab.

Additionally, we evaluated the feasibility of employing MnOHO-Ab

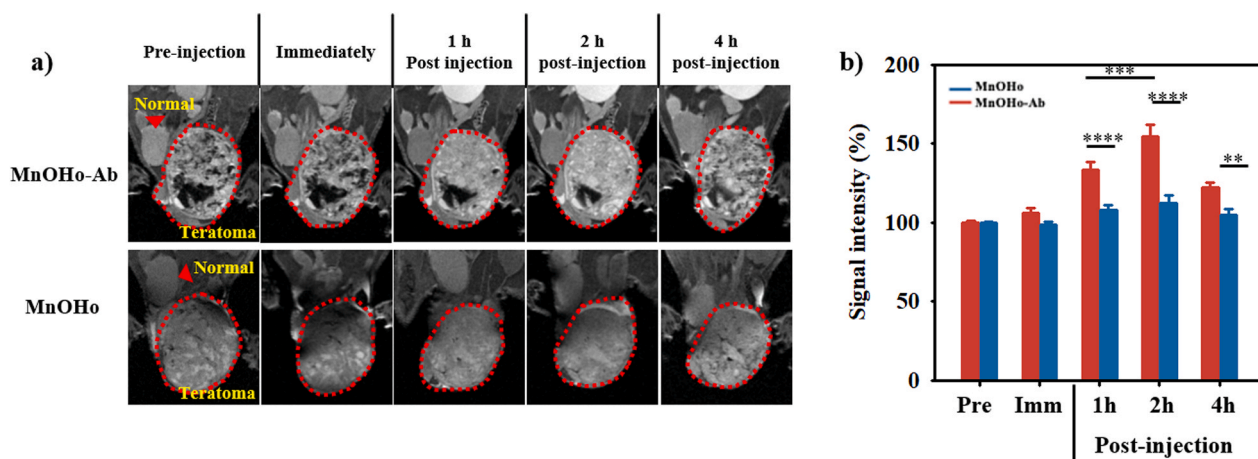


Fig. 4. Optimization of imaging time of MnOHO-Ab to monitor *in vivo* human stem cell transplantation. (a) *In vivo* T1-weighted MR images at different times (Pre-injection: before injection, Immediately: immediately following injection and 1, 2, and 4 h post-injection) after intravenous injection of MnOHO-Ab and MnOHO; The region within the red dashed line is the hiPSCs-induced teratoma area. (b) Relative T1 signal intensity (%) of the red-dashed line region of MRI images from a) (Signal intensity (%) = $\Delta R/R_{NT}$, where $\Delta R = R - R_{NT}$); Red bar and blue bar indicate MnOHO-Ab and MnOHO, respectively. For MRI images, 2 mg Mn was injected per mouse. Data represented is the mean \pm SD (** < 0.01, *** < 0.001, **** < 0.0001, two-way ANOVA with Tukey's tests). (For interpretation of the references to color in this figure legend, the reader is referred to the Web version of this article.)

as a T1 MRI probe for *in vivo* monitoring of stem cells by confirming its MR contrast effects. The T1- and T2-weighted MRI images acquired using a 3.0 T MRI scanner revealed concentration-dependent signal enhancement. As shown in Fig. 2h-i, MnOHO-Ab showed an increasingly strong and bright T1-weighted MRI image as the Mn ion concentration increased, which was calculated based on ICP-AES, accompanied by a higher relaxivity value as compared to commercial contrast media. The corresponding longitudinal relaxivity of MnOHO-Ab was measured based on T1- and T2-weighted MRI images. The T1 relaxivity (r_1) of MnOHO-Ab was $6.1 \text{ mM}^{-1}\text{s}^{-1}$, which was approximately 1.16–1.47 times higher than that of commercial T1 MRI contrast media (Magnevist®: $4.1 \text{ mM}^{-1}\text{s}^{-1}$ and Gadovist®: $5.2 \text{ mM}^{-1}\text{s}^{-1}$). The T2 relaxivity (r_2) of MnOHO-Ab was measured, based on T2-weighted MRI images, to calculate the r_2/r_1 ratio for evidence of the T1-MRI contrast agent, given that it was reported that the T1-MRI contrast agent had an r_2/r_1 ratio close to 1. In contrast, T2 contrast agents have a large r_2/r_1 ratio (>10) (Caspani et al., 2020; Hagberg and Scheffler 2013; Yin et al., 2018). MnOHO-Ab had an r_2/r_1 value of 1.57 (r_1 : $6.10 \text{ mM}^{-1}\text{s}^{-1}$ and r_2 : $9.57 \text{ mM}^{-1}\text{s}^{-1}$), which was close enough to 1, demonstrating the potential of MnOHO-Ab as a T1-MRI contrast agent. Moreover, there was no significant difference in r_1 , r_2 , and r_2/r_1 on comparing MnOHO (r_1 : $6.02 \text{ mM}^{-1}\text{s}^{-1}$, r_2 : $9.34 \text{ mM}^{-1}\text{s}^{-1}$ and r_2/r_1 : 1.55) and MnOHO-Ab. This indicated that the antibody present on MnOHO-Ab did not affect the T1 MR effect of MnOHO, and MnOHO-Ab had an excellent T1-weighted MR effect.

We have investigated *in vitro* effect of MnOHO-Ab on hiPSCs and MEFs. MEFs were used as control to show that MnOHO-Ab could distinguish hiPSCs from mouse cells prior to further *in vivo* investigation, and MnOHO-Ab could target only hiPSCs but not MEFs on *in vitro* analysis because MEFs were utilized as feeder cells on hiPSCs cultivation. The biocompatibility of MnOHO-Ab was evaluated on hiPSCs and MEFs using an MTT assay. Fig. 3a and S2a show that the toxicity of MnOHO-Ab in the presence of hiPSCs was negligible even at a significantly high concentration (10 mM), confirming that MnOHO-Ab can be applied as an *in vitro/in vivo* MRI contrast agent. We also observed that MnOHO-Ab could be internalized into the cytoplasm of hiPSCs in the short incubation time (1 h), whereas it did not internalize into that of MEFs (Fig. 3b and S2b). The cellular TEM images indicated that MnOHO-Ab could specifically target and bind to human cells (hiPSCs) due to the interaction between the antibody (Ab) and integrin $\beta 1$ on cells. The targeting ability of MnOHO-Ab was again assessed using a T1 MRI (Fig. 3c and d). hiPSCs and MEFs were treated with 2 mM and 10 mM MnOHO-Ab for 1 h, and their T1 MR images were compared with that of

non-treated cells, which were labeled as the control in Fig. 3c. As shown in Fig. 3c, the MnOHO-Ab-treated hiPSCs had a brighter T1 MR effect than that of MnOHO-Ab-treated MEFs due to specific binding between human cells and Ab. Based on T1-MRI images, each image's MR signal intensity was measured to evaluate the intensity ratio ($R = T^{-1}$) and the difference in intensity ratio between MnOHO-Ab-treated cells and non-treated cells ($\Delta R/R_{NT}$, where $\Delta R = R - R_{NT}$). The MR signal intensity ratio ($\Delta R/R_{NT}$ value) showed remarkable enhancement with MnOHO-Ab incubated hiPSCs. The 2 mM and 10 mM MnOHO-Ab incubated hiPSCs produced MR signal intensity ratio values of 76.3% and 223.0%, respectively (2 mM MnOHO-Ab treated hiPSCs: $76.3 \pm 11.6\%$ and 10 mM MnOHO-Ab treated hiPSCs: $223.0 \pm 21.2\%$). However, with MnOHO-Ab incubated MEFs, the MR signal intensity ratio was in the low range of 14.4–22.2% (2 mM MnOHO-Ab treated MEFs: $14.4 \pm 3.5\%$ and 10 mM MnOHO-Ab treated MEFs: $22.2 \pm 4.6\%$). Furthermore, the ratio value of 10 mM concentration on MEFs could not reach that value even for 2 mM concentration on hiPSCs (Fig. 3d). These results indicated that MnOHO-Ab could remarkably distinguish human stem cells in animal models with sensitive MR contrast effects and specific target abilities.

Before applying MnOHO-Ab to monitor *in vivo* human stem cells, the capability of MnOHO-Ab to detect human stem cells in an animal model, and the optimal *in vivo* MnOHO-Ab injection time was determined (Fig. 4). hiPSCs were transplanted into mouse testes, and the formation of teratomas was awaited. We observed T1-MRI images at various time intervals: pre-injection, immediately, 1, 2, and 4 h post intravenous injection of MnOHO-Ab as well as MnOHO. These data showed distinctly bright hiPSC-derived teratomas 1 h post-injection of the MnOHO-Ab compared to before the MnOHO-Ab injection. The teratoma site was gradually brightened for up to 2 h post-injection and became dark 4 h post-injection of MnOHO-Ab.

In contrast, MnOHO exhibited no significant difference in brightness on the hiPSC-derived teratomas at all experimental times. This result confirmed that MnOHO-Ab was effectively delivered and accumulated at the hiPSC-derived teratoma site by both antibody-mediated active targeting and enhanced permeability and retention effect-mediated passive targeting (Attia et al., 2019). Both uptake mechanisms helped MnOHO-Ab to effectively enter the teratoma and resulted in intense bright T1 images. From additional consideration of the MRI images of MnOHO that did not exhibit notable differences in brightness, we were able to discern that antibody-mediated active targeting was the preferred mechanism of MnOHO-Ab to detect human stem cells in an animal model, and it supported the capability of MnOHO-Ab for human

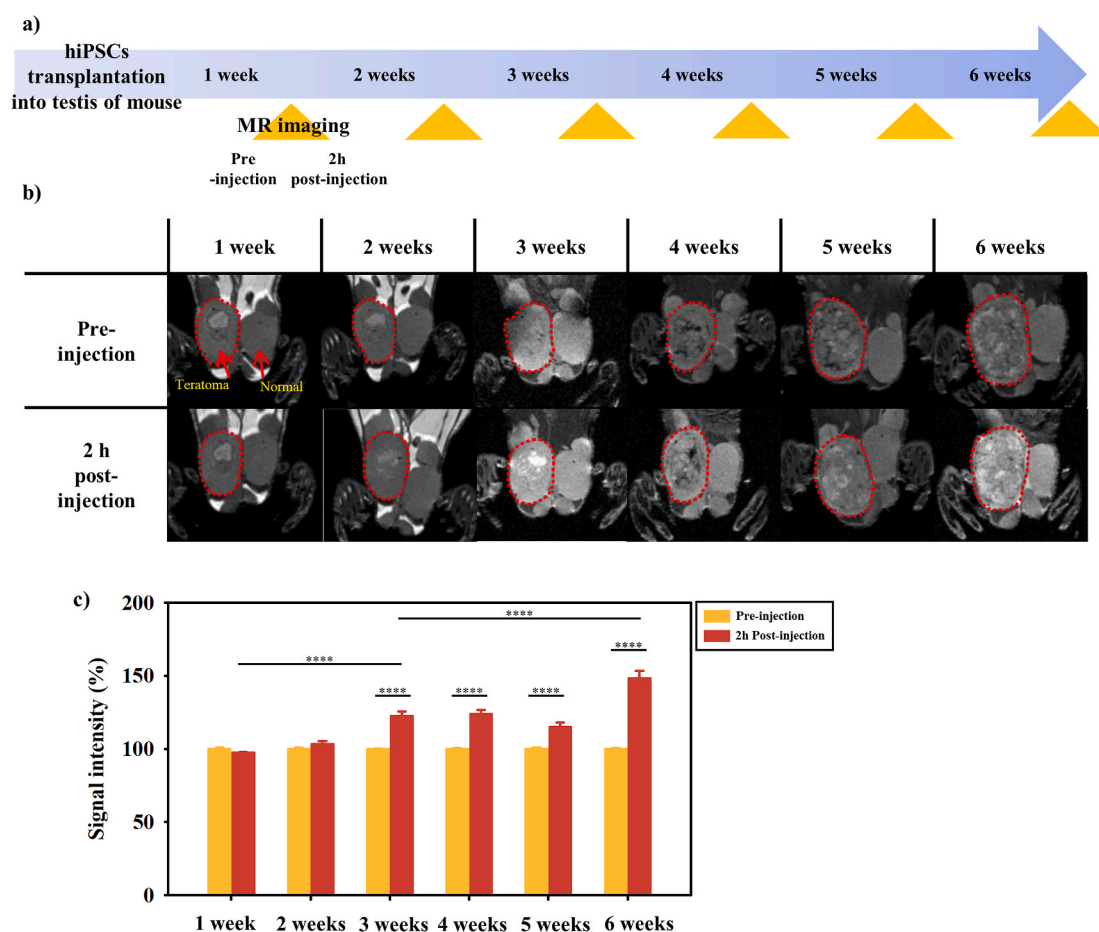


Fig. 5. Monitoring human stem cell transplantation of MnOHO-Ab at the pre-clinical level. (a) MRI schedule to monitor stem cell transplantation using MnOHO-Ab. A mouse was administered MnOHO-Ab. MRI images were captured every week after hiPSCs transplantation into the mouse testis. (b) *In vivo* T1-weighted MRI images after intravenous injection of MnOHO-Ab (2 mg Mn per injection), and (c) the relative T1 signal intensity (Signal intensity (%) = $\Delta R/R_{pre}$, where $\Delta R = R - R_{pre}$) of the region in the red dashed line. Orange and red bars represent T1 signal intensity of pre-injection and 2 h post-injection, respectively. Data represent mean \pm SD (** < 0.001 , **** < 0.0001 , two-way ANOVA with Tukey's test). (For interpretation of the references to color in this figure legend, the reader is referred to the Web version of this article.)

stem cell monitoring.

Moreover, signal intensity at the teratoma site 2 h post-injection of MnOHO-Ab increased by 54.2% (Signal intensity (%) = $R/R_{pre} \times 100$, Pre: Pre-injection) and decreased 4 h post-injection owing to the release of MnOHO-Ab from the teratoma. This implies that MnOHO-Ab does not have a long body-retention time, which has the advantage of biodegradation and lower risk of toxicity (El-Ansary and Al-Daihan 2009; Hoshyar et al., 2016; Wei et al., 2018). The main organs (brain, heart, kidney, liver, spleen, and testis) of the MnOHO-Ab injected mice were collected 2 days and 2 weeks after the MnOHO-Ab injection was administered and compared with that of non-injected mice to demonstrate whether MnOHO-Ab causes toxicity *in vivo*. Notably, the mice behaved normally without any noticeable signs of toxic side effects during the observation period after MnOHO-Ab administration. There were no apparent signs associated with organ damage or inflammatory lesions in mice 2 days and 2 weeks after the MnOHO-Ab treatment, as shown by H&E stained images for each organ of those mice (Fig. S4). This indicates that MnOHO-Ab is a good candidate for MRI contrast agents that can be safely used *in vivo*. Taken together, we confirmed the possibility and safety of MnOHO-Ab to trace *in vivo* human stem cells without *in vivo* toxicity and determined the optimal monitoring time of MnOHO-Ab at 2 h post-injection.

Finally, we applied MnOHO-Ab to monitor adoptively transferred human stem cells in an animal model (Fig. 5a). hiPSCs were transplanted into mice testes as a proof-of-concept model. The testes were monitored

during teratoma formation by T1-weighted MRI images with MnOHO-Ab every week since transplantation. Three weeks after transplantation, the difference in brightness and contrast gradually began to appear in the MRI images and was clearly observed at week six (Fig. 5b). The marginal T1 enhancement effect was observed until 3 weeks because the injected hiPSCs were not well-transplanted and were not integrated with peripheral blood vessels or tissues.

Since hiPSCs were engrafted in tissue, integrin $\beta 1$ expression would increase as cell adhesion and differentiation were in progress (Xiong et al., 2020). Then, MnOHO-Ab could trace hiPSCs through blood vessel migration and antibody-mediated targeting. Additionally, MR signals were measured and analyzed at the teratoma site (signal intensity (%) = $R_{2h}/R_{pre} \times 100$, Pre: Pre-injection, and 2 h: 2 h post-injection), and their intensity was gradually found to increase by 22.4%, 23.9%, 14.8%, and 48.4% for every week since week three (Fig. 5c). The data demonstrated that MnOHO-Ab could significantly detect and monitor hiPSCs in an animal model during hiPSC transplantation and engraftment.

Considering this result, together with short body retention time and unnoticeable toxicity in organs confirmed in Fig. 4 and S4, we concluded that MnOHO-Ab was able to safely monitor human stem cells' transplantation without *in vivo* toxicity. Additionally, we validated three germ layers in teratoma by histological analysis to demonstrate that MnOHO-Ab was not limited to one lineage of human stem cells. Fig. S5 shows the H&E stained image of teratoma-formed testis tissues at the six-week mark. Compared with the normal testis, the three germ layers

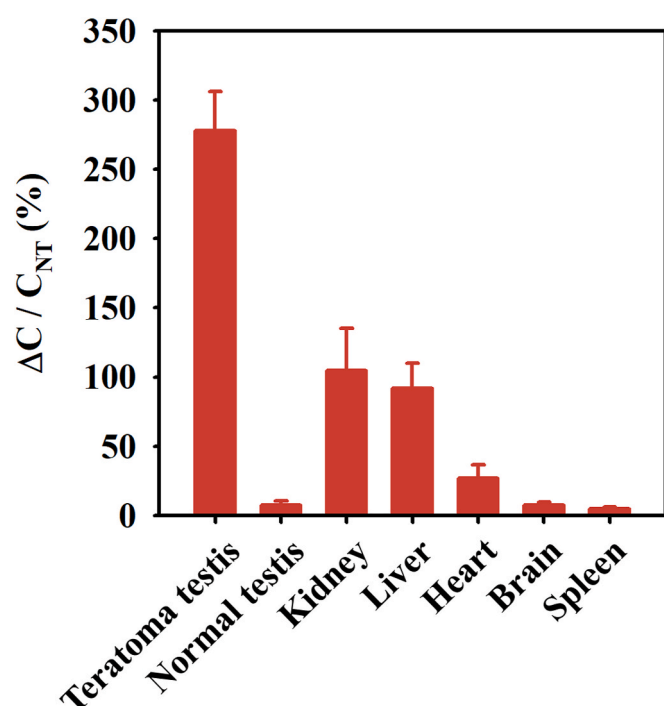


Fig. 6. Biodistribution of MnOHO-Ab. Relative concentrations of Mn^{2+} in the organs of a mouse treated with MnOHO-Ab compared to those in a non-treated mouse (NT).

comprising the ectoderm, mesoderm, and endoderm were clearly identified (Figs. S5 and S6). Taken together with the MRI image at week six in Fig. 5, MnOHO-Ab was verified to target three germ layers from hiPSCs because MnOHO-Ab overly brightened the hiPSC-derived teratoma on T1-weighted MRI images.

After the last MR monitoring at week six, the bio-distribution of manganese ions (Mn^{2+}) was confirmed by measuring the amount of Mn^{2+} distributed in each organ using ICP-AES analysis and organ weights (Fig. 6 and S7). As shown in Fig. 6, a dramatically large amount of Mn^{2+} accumulated in the hiPSC-derived teratoma compared to other organs, which was consistent with the results of *in vivo* MRI. Particularly, significantly higher concentrations of Mn^{2+} were measured in the hiPSC-derived teratoma than in the normal testis without the hiPSCs injection, which signified the targeting ability of MnOHO-Ab to trace and monitor human stem cells in an animal model.

We concluded that the MnOHO-Ab successfully targeted and monitored human stem cell lineage in an animal model without *in vivo* toxicity once the cells were integrated into the tissue. Consequently, MnOHO-Ab constitutes a promising T1-MRI contrast reagent, demonstrating the transplantation of adoptive transferred human stem cells at the pre-clinical stage of stem cell therapy.

4. Conclusions

This study proposes a new strategy for the MRI-mediated minimally invasive monitoring of *in vivo* stem cell therapy using MnOHO-Ab. The human integrin $\beta 1$ antibody, used to modify the MnOHO, enables MnOHO-Ab to specifically recognize the transplanted human stem cells at the pre-clinical level regardless of the stem cell-differentiation state.

In contrast to common approaches that needed stem cell-modification for monitoring transplanted stem cells in the pre-clinical stage, MnOHO-Ab has the advantages that it can be applied to monitor transplantation and tissue regeneration of most types of human stem cells without cell modification. Furthermore, this platform is expected to be applied to the technology for monitoring adoptive adult stem cell therapeutics for injured tissues.

CRedit authorship contribution statement

Seungmin Han: Formal analysis, Writing - original draft, designed the study, performed experiments, analyzed the results, and wrote the manuscript. **Byunghoon Kang:** Formal analysis, Writing - original draft, designed the study, performed experiments, analyzed the results, and wrote at the manuscript. **Hye Young Son:** performed *in vitro/in vivo* tests. **Yuna Choi:** performed *in vitro/in vivo* tests. **Moo-Kwang Shin:** performed the experiments. **Jongjin Park:** performed the experiments. **Jeong-Ki Min:** provided valuable suggestions and discussed the results. **Daewon Park:** provided valuable suggestions and discussed the results. **Eun-Kyung Lim:** conceived the idea and designed the study. **Yong-Min Huh:** conceived the idea and designed the study. **Seungjoo Haam:** conceived the idea and designed the study.

Declaration of competing interest

The authors declare that they have no known competing financial interests or personal relationships that could have appeared to influence the work reported in this paper.

Acknowledgments

This study was supported by the Bio & Medical Technology Development Program of the National Research Foundation (NRF) funded by the Ministry of Science & ICT (NRF-2018M3A9E2022819 and 2018M3A9E2022821), the Basic Science Research Program of the NRF funded by MSIT (NRF2018R1C1B6005424 and NRF-2017M3A9G5083322) the KRIBB Research Initiative Program. This research was supported by the Development of Measurement Standards and Technology for Biomaterials and Medical Convergence funded by the Korea Research Institute of Standards and Science (KRISS-2020-GP2020-0004).

Appendix A. Supplementary data

Supplementary data to this article can be found online at <https://doi.org/10.1016/j.bios.2021.113039>.

References

- Addisu, K.D., Hailemeskel, B.Z., Mekuria, S.L., Andrgie, A.T., Lin, Y.C., Tsai, H.C., 2018. ACS Appl. Mater. Interfaces 10, 5147–5160.
- Aime, S., Frullano, L., Geninatti Crich, S., 2002. Angew. Chem. Int. Ed. Engl. 41, 1017–1019.
- Ariza de Schellenberger, A., Kratz, H., Farr, T.D., Löwa, N., Hauptmann, R., Wagner, S., Taupitz, M., Schnorr, J., Schellenberger, E.A., 2016. Int. J. Nanomed. 11, 1517–1535.
- Attia, M.F., Anton, N., Wallyn, J., Omran, Z., Vandamme, T.F., 2019. J. Pharm. Pharmacol. 71, 1185–1198.
- Barsanti, C., Lenzarini, F., Kusmic, C., 2015. World J. Diabetes 6, 792–806.
- Bulte, J.W.M., Daldrup-Link, H.E., 2018. Radiology 289, 604–615.
- Caspani, S., Magalhães, R., Araújo, J.P., Sousa, C.T., 2020. Materials 13.
- Cen, P., Chen, J., Hu, C., Fan, L., Wang, J., Li, L., 2016. Stem Cell Res. Ther. 7, 143.
- Chen, S., Lewallen, M., Xie, T., 2013. Development 140, 255–265.
- Clark, A.Y., Martin, K.E., García, J.R., Johnson, C.T., Theriault, H.S., Han, W.M., Zhou, D. W., Botchwey, E.A., García, A.J., 2020. Nat. Commun. 11, 114.
- Doi, D., Magotani, H., Kikuchi, T., Ikeda, M., Hiramatsu, S., Yoshida, K., Amano, N., Nomura, M., Umekage, M., Morizane, A., Takahashi, J., 2020. Nat. Commun. 11, 3369.
- El-Ansary, A., Al-Daihan, S., 2009. J. Toxicol. 2009, 9. <https://doi.org/10.1155/2009/754810>, 754810.
- Hagberg, G.E., Scheffler, K., 2013. Contrast Media Mol. Imaging 8, 456–465.
- Hoshyar, N., Gray, S., Han, H., Bao, G., 2016. Nanomedicine 11, 673–692.
- Hwang, N.S., Varghese, S., Lee, H.J., Zhang, Z., Ye, Z., Bae, J., Cheng, L., Elisseeff, J., 2008. Proc. Natl. Acad. Sci. U.S.A. 105, 20641–20646.
- Idée, J.M., Port, M., Dencausse, A., Lancelot, E., Corot, C., 2009. Radiol. Clin. 47, 855–869.
- Ip, J.E., Wu, Y., Huang, J., Zhang, L., Pratt, R.E., Dzau, V.J., 2007. Mol. Biol. Cell 18, 2873–2882.
- Jarbak Nielsen, J.J., Lillethorup, T.P., Glud, A.N., Hedemann Sørensen, J.C., Orlowski, D., 2020. Acta Neurobiol. Exp. 80, 273–285.

- Kallas-Kivi, A., Trei, A., Stepanjuk, A., Ruisu, K., Kask, K., Pooga, M., Maimets, T., 2018. *Biol. Open* 7.
- Kukreja, A., Kang, B., Han, S., Shin, M.K., Son, H.Y., Choi, Y., Lim, E.K., Huh, Y.M., Haam, S., 2020. *Nano Converg* 7, 16.
- Li, L., Chen, X., Wang, W.E., Zeng, C., 2016. *Stem Cell. Int.* 9682757.
- Li, L., Guan, Q., Dai, S., Wei, W., Zhang, Y., 2017. *Front. Pharmacol.* 8, 135.
- Lian, Q., Zhang, Y., Zhang, J., Zhang, H.K., Wu, X., Lam, F.F., Kang, S., Xia, J.C., Lai, W. H., Au, K.W., Chow, Y.Y., Siu, C.W., Lee, C.N., Tse, H.F., 2010. *Circulation* 121, 1113–1123.
- Liu, L., Tseng, L., Ye, Q., Wu, Y.L., Bain, D.J., Ho, C., 2016. *Sci. Rep.* 6, 26271.
- Mathiasen, A.B., Qayyum, A.A., Jørgensen, E., Helqvist, S., Ekblond, A., Ng, M., Bhakoo, K., Kastrup, J., 2019. *Stem Cell. Int.* 2754927.
- McGinley, L.M., McMahon, J., Stocca, A., Duffy, A., Flynn, A., O'Toole, D., O'Brien, T., 2013. *Hum. Gene Ther.* 24, 840–851.
- Pan, D., Schmieder, A.H., Wickline, S.A., Lanza, G.M., 2011. *Tetrahedron* 67, 8431–8444.
- Panagiotopoulos, N., Duschka, R.L., Ahlborg, M., Bringout, G., Debbeler, C., Graeser, M., Kaethner, C., Lüdtke-Buzug, K., Medimagh, H., Stelzner, J., Buzug, T.M., Barkhausen, J., Vogt, F.M., Haegele, J., 2015. *Int. J. Nanomed.* 10, 3097–3114.
- Prowse, A.B., Chong, F., Gray, P.P., Munro, T.P., 2011. *Stem Cell Res.* 6, 1–12.
- Rajabzadeh, N., Fathi, E., Farahzadi, R., 2019. *Stem Cell Invest.* 6, 19.
- Rodriguez-Porcel, M., 2010. *Curr. Cardiol. Rep.* 12, 51–58.
- Santoso, M.R., Yang, P.C., 2016. *Stem Cell. Int.* 4198790.
- Shahror, R.A., Wu, C.C., Chiang, Y.H., Chen, K.Y., 2019. *JoVE* 153.
- Wang, P., Medarova, Z., Moore, A., 2011. *J. Transplant* 202915.
- Wei, Y., Quan, L., Zhou, C., Zhan, Q., 2018. *Nanomedicine* 13, 1495–1512.
- Won, Y.W., Patel, A.N., Bull, D.A., 2014. *Biomaterials* 35, 5627–5635.
- Xiong, S., Xu, Y., Wang, Y., Kumar, A., Peters, D.M., Du, Y., 2020. *Stem Cell. Dev.* 29, 290–300.
- Yin, X., Russek, S.E., Zabow, G., Sun, F., Mohapatra, J., Keenan, K.E., Boss, M.A., Zeng, H., Liu, J.P., Viert, A., Liou, S.H., Moreland, J., 2018. *Sci. Rep.* 8, 11863.
- Zakrzewski, W., Dobrzyński, M., Szymonowicz, M., Rybak, Z., 2019. *Stem Cell Res. Ther.* 10, 68.
- Zhang, M., Methot, D., Poppa, V., Fujio, Y., Walsh, K., Murry, C.E., 2001. *J. Mol. Cell. Cardiol.* 33, 907–921.